CARBON 50 (2012) 1614–1618

Available at www.sciencedirect.com

SciVerse ScienceDirect

journal homepage: www.elsevier.com/locate/carbon

Extinction of ferromagnetism in highly ordered pyrolytic graphite by annealing

Xiaochang Miao [a], *Sefaattin Tongay* [a,b], *Arthur F. Hebard* [a,*]

[a] *Department of Physics, University of Florida, Gainesville, FL 32611, United States*
[b] *Department of Material Science and Engineering, University of Florida, Gainesville, FL 32611, United States*

ARTICLE INFO

Article history:
Received 17 June 2011
Accepted 22 November 2011
Available online 29 November 2011

ABSTRACT

We report that the ferromagnetism of highly ordered pyrolytic graphite (HOPG) samples as measured by hysteretic magnetization loops can be diminished and eventually extinguished with sufficiently long high vacuum anneals at temperatures on the order of 2300 °C. Concomitant with the extinction of ferromagnetism, we observe an anneal-induced increase in grain size (accompanied by possible edge reconstruction) confirmed by X-ray diffraction measurements and improved transport properties, including lower in-plane and out-of-plane resistivity, higher electron and hole mobility and improved charge compensation. The implied reduction of defects and vacancies by annealing suggests that the ferromagnetism of pristine HOPG is correlated with localized states located at zigzag edges, vacancies and related defects.

1. Introduction

Although high quality graphite has been studied for more than four decades, many of its fundamental physical properties, such as out-of-plane electronic transport, magnetoresistive properties and intrinsic ferromagnetism, have yet to be fully understood. In particular, observations of ferromagnetism (FM) in highly ordered pyrolytic graphite (HOPG) crystals that are known to be free of magnetic transition metal impurities [1,2] are particularly puzzling and have generated vigorous research activity to clarify possible physical mechanisms. The present consensus on the origin FM in graphene/graphite is that the magnetism is mainly associated with defects such as vacancies by creating dangling bonds, and zigzag edges by inducing spin polarization via electron–electron interactions [3,4]. This consensus is supported by scanning tunneling microscopy experiments on single atom vacancies on graphite surfaces [5] and the increase in magnetism associated with irradiation of graphite by protons [6], carbon atoms [7,8] and helium ions [9]. The linear temperature dependence of the magnetization [6] suggests that the magnetization of proton-bombarded graphite has a two-dimensional (2D) graphene-like character possibly related to 2D periodic networks of point defects [2]. This is also consistent with the anisotropic FM in low-dose helium irradiated graphite where the defects, induced by a chemically inert implant, mainly locate on the grain boundaries propagating along *c* axis [9].

In spite of the current understanding of the contribution from zigzag edges and defects [3,4], questions about the origins of FM still assume a broader perspective. Accordingly, further explorations on this subject are continuously in progress, especially since spurred by recently discovered techniques to obtain single layer sheets of graphene [10] or graphene derivatives. For example magnetization studies of sonically exfoliated graphene nanocrystals show no evidence of ferromagnetism [11] whereas partially hydrogenated epitaxial graphene shows room-temperature ferromagnetism that is believed to be associated with unpaired electrons occupying the remnant delocalized π bonding network [12]. To fully understand the physical mechanisms for magnetism in

* *Corresponding author:* Fax: +1 352 392 3591.
E-mail address: afh@phys.ufl.edu (A.F. Hebard).
0008-6223/$ - see front matter
doi:10.1016/j.carbon.2011.11.040

both graphite and graphene [4], the role of dimensionality needs more theoretical and experimental work. Dimensionality considerations apply to finite graphene nanostructures, to graphene nanoribbons with armchair or zigzag edges, to graphene with magnetism induced by the presence of defects or chemical modifications and to proton-irradiated graphite [6,13] where the interaction between hydrogen and surface carbon atoms is important [13].

In this paper, rather than focusing on efforts to enhance ferromagnetism in HOPG, we report that annealing of HOPG under high vacuum conditions diminishes ferromagnetism in a controlled and reproducible manner. At sufficiently high temperatures, ferromagnetism is extinguished altogether. The magnetic samples are annealed for varying times to temperatures as high as 2300 °C and results correlated with measurements of magnetization, hysteresis, crystalline quality by X-ray diffraction (XRD), Raman spectra and electrical transport. Our central result is that the anneal-induced reduction of the saturation magnetization (M_s) from its original value to zero (non-ferromagnetic) is accompanied by an improvement in electrical properties and crystallinity, thereby implying that defect-free HOPG is inherently non-ferromagnetic. Our results support the notion that any FM background signal in chemically pure HOPG is associated with defects which at sufficiently high temperature can be annealed out or effectively neutralized. The relevant defects appear to be grain boundaries with zigzag edges and single/multi-atom vacancies but might also include dislocations and interstitial bridging atoms between neighboring graphene layers.

2. Experimental procedure

Our graphite samples are cut from highly oriented pyrolytic graphite (HOPG) pieces with 0.4–3.4° mosaic spread and in-plane resistivity ρ_{ab} spanning a 4–45 μΩ cm range at room temperature. Electronic transport measurements were performed on a Hall bar contact configuration mounted in a physical property measurement system (PPMS) and measured using a 17 Hz AC resistance bridge to temperatures as low as 5 K and magnetic fields H up to 70 kOe. The magnetization $M_\perp$ was measured in a superconducting quantum interference device (SQUID) in the same temperature range and in magnetic fields applied perpendicular to the c-axis. In this direction, the magnitude of the magnetic susceptibility $\chi_\perp^{dia}$ is more than an order of magnitude lower than the susceptibility $\chi_\parallel^{dia}$ found when H is applied parallel to the c-axis, thus allowing the background diamagnetic signal to be minimized. The HOPG samples were annealed in a high vacuum ($\sim 5\times10^{-7}$ Torr) chamber by Joule heating, i.e., by passing a direct current of ~200–260 A through a flat tungsten boat in thermal contact with the HOPG samples. The annealing temperature was measured using a C-type thermocouple and kept between 2100 and 2300 °C for ~5–6 min. Pristine and annealed samples were characterized using X-ray diffraction (XRD) and Raman spectroscopy. XRD patterns were collected with a Philips diffractometer using Cu-Kα radiation in a θ–2θ configuration and the Raman spectra were measured from 1200 to 3000 cm^{-1} using a green (532 nm) light source.

3. Results and discussion

Fig. 1 shows $M_\perp$ vs H data (black squares) at 5 K (a) before and (b) after subtracting the diamagnetic background ($M_\perp^{Dia}$) signal on the same sample. Prior to the heat treatment, HOPG samples give typical mass susceptibilities $\chi_\perp^{dia}$ in the range -5.0×10^{-7} to -8.5×10^{-7} emu g^{-1} Oe^{-1} consistent with values reported in the literature [2,14]. However, based on the data taken from 11 HOPG samples with different mosaic spread range (more specifically, 2 samples with 0.4° spread, 1 sample with 0.5° spread, 2 samples with 0.7° spread, 1 sample with 0.9° spread and 5 samples with 3.4° spread), we have found that the measured saturated moment (M_s) values differ noticeably for samples with different mosaic spread without any obvious correlation between mosaic spread and M_s. This might be attributed to different total grain boundary areas and defect densities within the HOPG crystal that are uncorrelated with crystalline quality, i.e., mosaic spread as determined by X-ray rocking curves.

After the magnetization measurements, the same sample was then annealed up to 2100 °C for 5 min and then slowly cooled to room temperature before reloading into the SQUID for more magnetization measurements. We observed that annealed HOPG becomes less FM, i.e., M_s decreases by 60–70%. Annealing the same sample for another 5 min up to 2300 °C extinguishes all signs of ferromagnetism and the diamagnetic response (straight line with negative slope) dominates (Fig. 1a

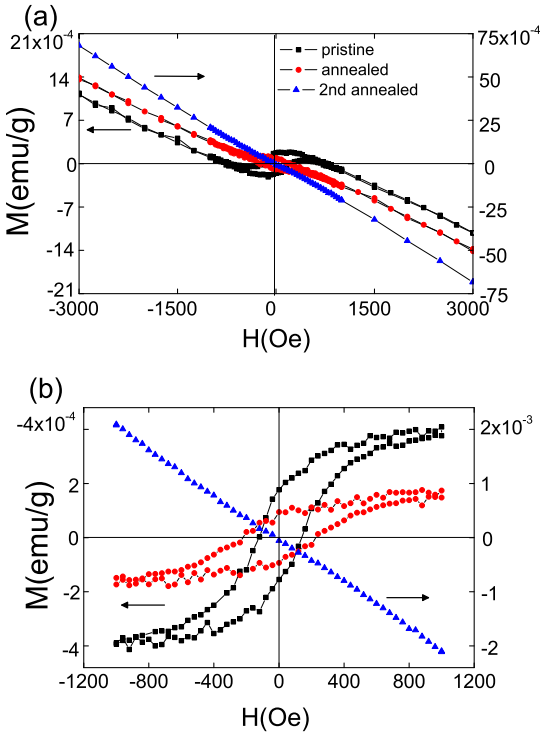

Fig. 1 – (a) $M_\perp$ vs H measured at 5 K in pristine HOPG (black squares), after annealing to 2100 °C (red circles), and up to 2300 °C (blue triangles) for 5 min in high vacuum. (b) $M_\perp$ vs H loops after subtracting the diamagnetic background signal. (For interpretation of the references to color in this figure legend, the reader is referred to the web version of this article.)

and b). We note from the three traces of Fig. 1a that the diamagnetic susceptibility $\chi_{\perp}^{dia}$ of the pristine ferromagnetic sample increases by a factor of four from -4.98×10^{-7} for the pristine ferromagnetic sample to -2.04×10^{-6} emu g^{-1} Oe^{-1} for the fully annealed non-ferromagnetic sample. Similar trends have been observed for intercalated graphite compounds which have a smaller diamagnetic susceptibility than pristine graphite [15].

To further understand the effect of annealing on the magnetization properties of HOPG, we measured X-ray diffraction (XRD) and Raman spectra of pristine and annealed samples (Fig. 2a and b). The XRD patterns of the HOPG samples display sharp (002) and (004) peaks, as expected. In the inset to Fig. 2, we display expanded views of the (004) peaks before and after annealing. As shown by the arrows, the full width half maximum (FWHM) of the (004) peak decreases after annealing. Inserting the observed peak widths of the XRD signal into Scherrer's formula, we find that the average grain size increases by ~30% after annealing, in agreement with anneal-induced crystallite size increases observed in previous work [16].

In Fig. 2b we show Raman spectra of the samples before and after annealing, and in the inset we show three main features, i.e, the G and 2D peaks. The observed G peak can be attributed to the bond stretching of sp^2 bonded carbon in the graphite while the graphite 2D peak, consisting of $2D_1$ and $2D_2$ components, is a reflection of second order scattering from lattice imperfection with particular sensitivity to the stacking order of graphene sheets along the c axis (Fig. 2b inset). Additionally, our HOPG samples do not display noticeable disorder D peaks (at 1350 cm^{-1}), which are due to the first-order scattering by the defects. The ratio of intensity of the D peak to that of the G peak (I_D/I_G) is inversely proportional to the in-plane crystalline size [9,16]. However, in contrast to the evolution of the D peak with increasing disorder as shown by previous work on polycrystalline graphite [17] and on helium ion bombarded HOPG samples with varying doses [9], the absence of D peaks in our case indicates that the HOPG samples are free of disorder within the detection of Raman spectroscopy and does not allow us to probe the density of disorder (*e.g.* vacancies, broken bonds, dislocations and concentration of amorphous carbon). Overall, Raman spectra taken on pristine and annealed samples do not show noticeable differences. Unlike XRD measurements, no conclusion can be drawn from Raman spectroscopy.

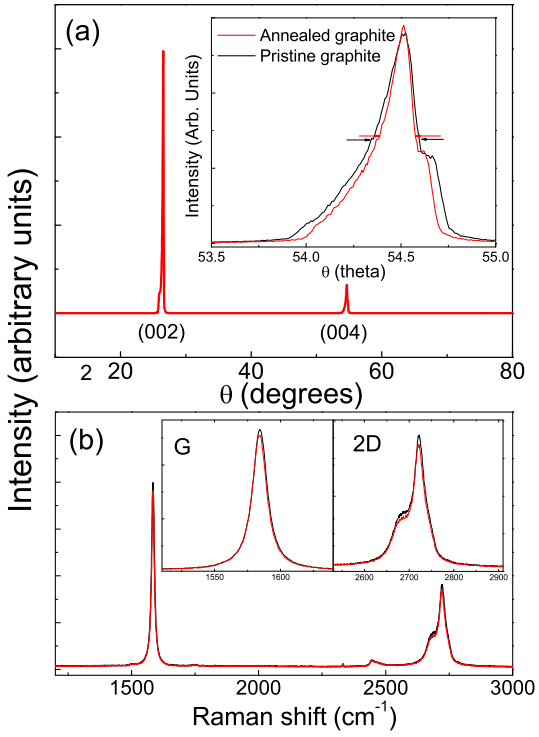

Fig. 2 – (a) XRD pattern of pristine and annealed HOPG displaying (002) and (004) reflections. Inset: expanded view of the (004) reflection on pristine (black curve) and annealed (red curve) HOPG. The width of the (004) peak at the FWHM of the pristine HOPG (black arrows) decreases after annealing (red arrows). (b) Raman spectra of pristine and annealed HOPG with 532 nm laser. Inset: detailed Raman spectrum around G and 2D peak regions. (For interpretation of the references to color in this figure legend, the reader is referred to the web version of this article.)

Our observed anneal-induced improvement in crystalline quality accompanying the extinction of ferromagnetism is consistent with the theoretical consensus that in defected graphite a large number of zigzag edges with carbene-like triplet ground states [3] along the grain boundaries play an important role in understanding the underlying ferromagnetic behavior [4]. As suggested in previous work [16,18,19], zigzag edges break the symmetry of the graphene sublattice and give rise to localized electron states near the Fermi level. The repulsive electron–electron interactions are responsible for the spin polarization and the unexpected ferromagnetism in graphene/graphite [20–23]. However, as shown from density functional theory and first principle calculations, the zigzag edge may be metastable [16,18,20,24], and planar armchair-like edge reconstruction (a combination of one pentagon and one heptagon) is possible even at room temperature [18]. This zigzag to armchair reconstruction process will greatly depress the FM signal [20].

At the same time, chemisorption of oxygen is possible around the edges (especially zigzag edges) [3] and heat treatment above 200 °C will remove those oxygen atoms as found in graphene oxides (GO) [25]. However, in HOPG the oxygen ratios are undetectable in contrast to induced oxygen in GOs. Furthermore, annealing HOPG above 2100 °C is close to the graphitization temperature (⩾2400 °C), thus not only high enough to remove absorbed oxygen atoms, if there are any, but also able to expand the crystallite size by restoring the C bonding at the grain boundaries [16] as confirmed by XRD measurement. Additional consequences of the annealing process include removal of the mono/multi vacancies [26] and/or triggering edge reconstruction, thereby increasing the density of reconstructed edges at grain boundaries.

It is reasonable to expect that most if not all of the above-mentioned will improve the electrical properties of the HOPG. This expectation is borne out by our electrical measurements performed on pristine and annealed HOPG samples which show that the in-plane room-temperature resistivity $\rho_{ab}^{300\ K}$ can decrease (Fig. 3a) by a factor of more than five. If for

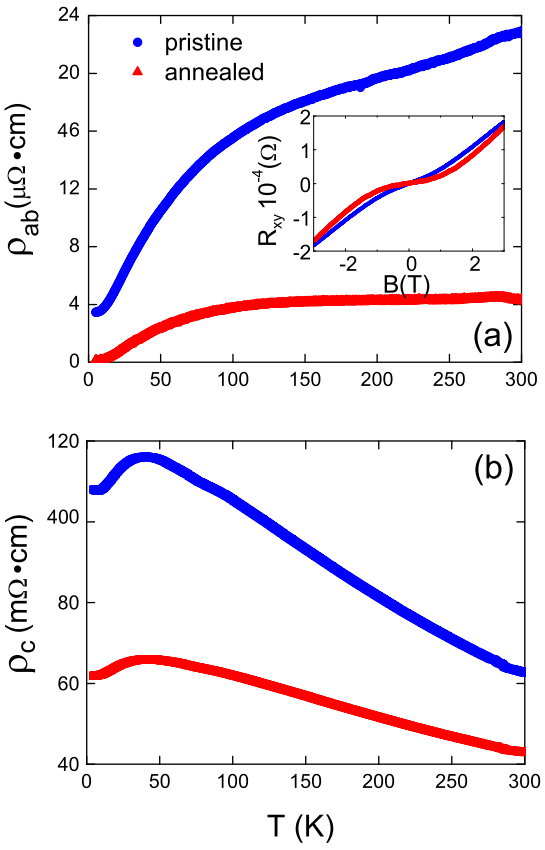

Fig. 3 – Temperature dependence of (a) in-plane resistivity (ρ_{ab}) and (b) out-of-plane resistivity (ρ_c) before (blue circles) and after (red triangles) the annealing. Inset: hall resistivity ρ_{xy} vs magnetic induction field (B) before and after the annealing. (For interpretation of the references to color in this figure legend, the reader is referred to the web version of this article.)

simplicity we assume that the carrier density n is fixed, then the Drude model predicts that the decrease in $\rho_{ab}^{300\ K}$ implies an overall ~5 times increase in mobility μ. A constant n approximation is however not valid as shown by Hall effect data discussed in the next paragraph, since most of the carriers derive from unintentional impurities in HOPG as well as from localized states at the Fermi level caused by defect sites/grain boundaries. Therefore, grain boundaries have higher charge density than bulk [27]. However, at high temperature those edge-localized charges have an increased chance to become delocalized because of restored C bonding across the boundaries. This increased contribution to the number of free carriers after annealing is also consistent with the enhanced diamagnetic background signal in annealed HOPG described previously and shown in Fig. 1(a).

The temperature dependence of the in-plane ρ_{ab} and out-of-plane ρ_c resistivity of two separate samples cut from the same piece is shown in panels (a) and (b) of Fig. 3. These data display the well known large resistance anisotropy of graphite and also confirm that, over the entire 5–300 K temperature range, the resistance of annealed HOPG is significantly less than the resistance of pristine HOPG. The in-plane conductivity of graphite is dominated by electrons and holes with comparable carrier densities n_e and n_h but different mobilities μ_e and μ_h, respectively. Hall data (see inset Fig. 3a) taken at 300 K show that the low-field slope (carrier density) of the annealed sample is lower (higher) when compared to the pristine sample. Employing a two-band model [28] to analyze $\rho_{ab}(T)$ in conjunction with the Hall data we extract $\mu_h =$ 3120 cm^2/V s(6900 cm^2/V s), $\mu_e =$ 8350 cm^2/V s (11, 900 cm^2/V s), $n_h = 7.53 \times 10^{19}$ cm^{-3} (1.26×10^{20} cm^{-3}) and $n_e = 4.64 \times 10^{18}$ cm^{-3} (4.17×10^{19} cm^{-3}) for the pristine and annealed samples respectively. Although both n_e and n_h increase after annealing, we find that the compensation, $(n_h - n_e)/(n_h + n_e)$, decreases from 0.884 before annealing to 0.503 after annealing. Thus annealing not only delocalizes trapped charge at defects but also brings the HOPG closer to perfect compensation where the electron and carrier densities are equal. In addition, the decrease in $\rho_{ab}^{300\ K}$ and corresponding increase in μ_e and μ_h indicate that annealing decreases the overall resistivity by restoring C bonding at grain boundaries while simultaneously removing scattering centers, which is equivalent to annealing out vacancies and defects.

However, the decrease of ρ_c cannot be explained since the dominant transport process in the c-axis direction is still under debate and remains elusive. Nevertheless, we note that the temperature where ρ_c gives a maximum peak (T_{max}) shifts from 40 to 42 K after annealing but does not disappear. Existence of the peak at T_{max} even after annealing up to 2100 °C implies that the non-monotonic temperature dependence (and hence T_{max}) may be a fundamental feature of graphite, or may be associated with various other process such as stacking-fault interlayer charge transfer and tunneling conduction through the stacking disorders as discussed in previous works [15,29].

4. Conclusions

We have demonstrated that the ferromagnetism of HOPG crystals can be extinguished by annealing under high vacuum conditions at high temperature. Coincident with the annealing and the disappearance of hysteretic magnetization loops there is a crystallite size increase, an increase in diamagnetism, a decrease in resistivity in both the in-plane and out-of-plane directions and a decrease in carrier compensation. Our results suggest that unless ferromagnetic transition metal impurities are present, the FM originates solely from grain boundaries, edge defects and/or vacancies. A perfect chemically pure HOPG crystal without defects will not exhibit ferromagnetic behavior. We attribute the anneal-induced FM-to-diamagnetic transition to a reconfiguration of broken C bonds (defects) at the grain boundaries (as confirmed by an increase in overall mobility by electronic transport measurements) as well as to possible zigzag edge reconstruction to achieve more stable but non-ferromagnetic armchair configurations. Our study not only provides more insight into the nature of FM in HOPG but also allows one to tune the magnetization properties of intentionally defected ferromagnetic HOPG to achieve better spintronic properties, longer spin coherence length or overall higher mobility.

Acknowledgements

This work is supported by the National Science Foundation (NSF) under Contract Number 1005301 (AFH) and by the Office of Naval Research (ONR) under Contract Number 00075094 (ST). The authors appreciate useful discussions with Bill Appleton and technical support by the Nanoscience Institute for Medical and Engineering Technology at the University of Florida.

REFERENCES

[1] Esquinazi P, Setzer A, Hohne R, Semmelhack C, Kopelevich Y, Spemann D, et al. Ferromagnetism in oriented graphite samples. Phys Rev B 2002;66(2):024429-1–10.
[2] Cervenka J, Katsnelson MI, Flipse CFJ. Room-temperature ferromagnetism in graphite driven by two-dimensional networks of point defects. Nature Phys 2009;5(11):840–4.
[3] Radovic LR, Bockrath B. On the chemical nature of graphene edges: origin of stability and potential for magnetism in carbon materials. J Am Chem Soc 2005;127(16):5917–27.
[4] Yazyev OV. Emergence of magnetism in graphene materials and nanostructures. Rep Prog Phys 2010;73(5):1–18.
[5] Ugeda MM, Brihuega I, Guinea F, Gomez-Rodriguez JM. Missing atom as a source of carbon magnetism. Phys Rev Lett 2010;104(9):096804-1–4.
[6] Barzola-Quiquia J, Esquinazi P, Rothermel M, Spemann D, Butz T, Garcia N. Experimental evidence for two-dimensional magnetic order in proton bombarded graphite. Phys Rev B 2007;76(16):161403-1–4.
[7] Xia HH, Li WF, Song Y, Yang XM, Liu XD, Zhao MW, et al. Tunable magnetism in carbon-ion-implanted highly oriented pyrolytic graphite. Adv Mater 2008;20(24):4679–83.
[8] Lee H, Miyamoto Y, Yu JJ. Possible origins of defect-induced magnetic ordering in carbon-irradiated graphite. Phys Rev B 2009;79(12):121404-1–4.
[9] Makarova TL, Shelankov AL, Serenkov IT, Sakharov VI, Boukhvalov DW. Anisotropic magnetism of graphite irradiated with medium-energy hydrogen and helium ions. Phys Rev B 2011;83(8):085417-1–8.
[10] Novoselov KS, Geim AK, Morozov SV, Jiang D, Zhang Y, Dubonos SV, et al. Electric field effect in atomically thin carbon films. Science 2004;306(5696):666–9.
[11] Sepioni M, Nair RR, Rablen S, Narayanan J, Tuna F, Winpenny R, et al. Limits on intrinsic magnetism in graphene. Phys Rev Lett 2010;105(20):207205-1–4.
[12] Xie L, Wang X, Lu J, Ni Z, Luo Z, Mao H, et al. Room temperature ferromagnetism in partially hydrogenated epitaxial graphene. App Phys Lett 2011;98(19):193113-1–3.
[13] Ohldag H, Esquinazi P, Arenholz E, Spemann D, Rothermel M, Setzer A, et al. The role of hydrogen in room-temperature ferromagnetism at graphite surfaces. New J Phys 2010;12:123012-1–10.
[14] Heremans J, Olk CH, Morelli DT. Magnetic susceptibility of carbon structures. Phys Rev B 1994;49(21):15122–5.
[15] Dresselhaus MS, Dresselhaus G. Intercalation compounds of graphite. Adv Phys 1981;30(2):139–326.
[16] Pimenta MA, Dresselhaus G, Dresselhaus MS, Cancado LG, Jorio A, Saito R. Studying disorder in graphite-based systems by Raman spectroscopy. Phys Chem Chem Phys 2007;9(11):1276–91.
[17] Tuinstra F, Koenig KL. Raman spectrum of graphite. J Chem Phys 1970;53(3):1126–30.
[18] Koskinen P, Malola S, Hakkinen H. Self-passivating edge reconstructions of graphene. Phys Rev Lett 2008;101(11):115502-1–4.
[19] Makarova TL. Magnetic properties of carbon structures. Semiconductors 2004;38(6):615–38.
[20] Song LL, Zheng XH, Wang RL, Zeng Z. Dangling bond states, edge magnetism, and edge reconstruction in pristine and B/N-terminated zigzag graphene nanoribbons. J Phys Chem C 2008;114(28):12145–50.
[21] Vozmediano MAH, Lopez-Sancho MP, Stauber T, Guinea F. Local defects and ferromagnetism in graphene layers. Phys Rev B 2005;72(15):155121-1–5.
[22] Lee H, Son YW, Park N, Han SW, Yu JJ. Magnetic ordering at the edges of graphitic fragments: magnetic tail interactions between the edge-localized states. Phys Rev B 2005;72(17):174431-1–8.
[23] Nakada K, Fujita M, Dresselhaus G, Dresselhaus MS. Edge state in graphene ribbons: nanometer size effect and edge shape dependence. Phys Rev B 1996;54(24):17954–61.
[24] Huang B, Liu M, Su N, Wu J, Duan W, Gu B-l, et al. Quantum manifestations of graphene edge stress and edge instability: a first-principles study. Phys Rev Lett 2009;102(16):166404-1–4.
[25] Pan DP, DY, Zhang JC, Li Z, Wu MH. Hydrothermal route for cutting graphene sheets into blue-luminescent graphene quantum dots. Adv Mater 2010;22(6):734.
[26] Yang XM, Xia HH, Qin XB, Li WF, Dai YY, Liu XD, et al. Correlation between the vacancy defects and ferromagnetism in graphite. Carbon 2009;47(5):1399–406.
[27] Cervenka J, Flipse CFJ. Structural and electronic properties of grain boundaries in graphite: planes of periodically distributed point defects. Phys Rev B 2009;79(19):195429.
[28] Du X, Tsai SW, Maslov DL, Hebard AF. Metal-insulator-like behavior in semimetallic bismuth and graphite. Phys Rev Lett 2005;94(16):166601-1–4.
[29] Matsubara K, Sugihara K, Tsuzuku T. Electrical-resistance in the C-direction of graphite. Phys Rev B 1990;41(2):969–74.